

Article

FeC₄H₂²⁺ Encompassing Planar Tetracoordinate Iron: Structure and Bonding Patterns

Shilpa Shajan¹, Kandasamy Thirunavukkarasu², Vijayanand Chandrasekaran^{1,*},
Venkatesan S. Thimmakonda^{3,*} and Krishnan Thirumoorthy^{1,*}

¹ Department of Chemistry, School of Advanced Sciences, Vellore Institute of Technology, Vellore 632014, India; shilpa.shajan2020@vitstudent.ac.in

² Vel Tech Rangarajan Dr Sagunthala R&D Institute of Science and Technology, Avadi, Chennai 600062, India; drkthirunavukkarasu@veltech.edu.in

³ Department of Chemistry and Biochemistry, San Diego State University, San Diego, CA 92182-1030, USA

* Correspondence: vijayanand.c@vit.ac.in (V.C.); vthimmakondusamy@sdsu.edu (V.S.T.); thirumoorthy.krishnan@vit.ac.in (K.T.)

Abstract: The singlet, triplet, and quintet electronic states of the FeC₄H₂²⁺ system are theoretically explored using quantum chemical methods, and 39 isomers are identified in the singlet electronic state and 4 isomers in both triplet and quintet electronic states. A molecule with a planar tetracoordinate iron (ptFe) is found on the potential energy surface of singlet and triplet electronic states. The bonding features of ptFe in the singlet electronic state are analyzed with natural bond orbital (NBO) analysis, adaptive natural density partitioning (AdNDP), and molecular orbital analysis. The resultant data delineate that the ptFe is stabilized through electron delocalization in the ptFe system.

Keywords: FeC₄H₂²⁺; planar tetracoordinate iron; delocalization; computational chemistry



Citation: Shajan, S.; Thirunavukkarasu, K.; Chandrasekaran, V.; Thimmakonda, V.S.; Thirumoorthy, K. FeC₄H₂²⁺ Encompassing Planar Tetracoordinate Iron: Structure and Bonding Patterns. *Atoms* **2024**, *12*, 11. <https://doi.org/10.3390/atoms12020011>

Academic Editor: Kirill Tuchin

Received: 28 December 2023

Revised: 7 February 2024

Accepted: 14 February 2024

Published: 18 February 2024



Copyright: © 2024 by the authors. Licensee MDPI, Basel, Switzerland. This article is an open access article distributed under the terms and conditions of the Creative Commons Attribution (CC BY) license (<https://creativecommons.org/licenses/by/4.0/>).

1. Introduction

The study of transition metal clusters, especially first-row transition metal clusters, has sparked the interest of several research groups over the years due to the clusters' unique structural, electronic, magnetic, and catalytic properties [1–5]. Iron (Fe) is one of the universe's most prevalent heavy and refractory elements. Iron–carbon clusters have provided an in-depth understanding of geometrical properties, electronic structures, and magnetism among the transition metal clusters because of iron's position between early and late transition metals due to experimental measurements [6–8] and theoretical calculations [9–11]. Experimental studies on the iron–carbon clusters include mass spectrometry, infrared isolation matrix spectrometry, anion photoelectron spectroscopy, and gas-phase ion chromatography [7,8,12–16]. FeC_n (n ≤ 8) [17–20] and Fe_nC (n ≤ 13) [21–23] iron–carbon clusters have been theoretically examined in the past, and some of them have been reported experimentally [24]. The clusters of iron, carbon, and hydrogen have also been the subject of similar studies. In 1987, for the first time, neutral FeCH_n (n = 0–3) systems were produced and characterized in the gas phase by Schwarz et al. using neutralization–reionization mass spectrometry (NRMS) [25]. Fan et al. have investigated FeC_n and FeC_nH (n = 2) clusters via anion photoelectron spectroscopy [26]. The cation of the FeCH₂ cluster was also investigated experimentally via photofragment spectroscopy [27]. In 2003, Boesl et al. identified the FeC₄H₂ neutral complex experimentally using mass selective photo-detachment photoelectron spectroscopy [28]. In 2013, Chandra and coworkers conducted studies on the molecular and spectroscopic properties of iron-containing ring molecules, including theoretical studies on cyclic compounds like FeC₂, FeC₃, FeC₃H₂, FeC₂H₂, FeC₂H₄, and FeC₃H₄, which are of astrophysical interest [29]. Transition metal clusters have gained potential applications in various fields since the discovery of metallocarbohedrene in 1992 [30]. The list extends from materials to the emerging field of

nanotechnology and also exhibits remarkable applications in organic chemistry [16,31–34]. A prominent instance is the challenging activation of methane by iron carbide cluster ions [5,35]. Another interesting application of these compounds is their catalytic activity in oxygen reduction, CO_x ($x = 1, 2$) reduction, and also in Fischer–Tropsch synthesis [36–39]. Energy and hydrogen storage are further applications of these compounds [40–43]. The prospective applications of these iron–carbon clusters extend beyond material science; other significant areas include surface chemistry, astrochemistry, and combustion chemistry.

On the other hand, there have been extensive studies on aberrant molecules that deviate from the accepted notions in chemistry ever since H. J. Monkhorst proposed the concept of planar tetracoordinate carbon (ptC) in 1968 [44]. In 1970, Hoffman and co-workers proposed ways to stabilize the ptC [45], which in turn spurred unremitting experimental and computational investigations into “planar hypercoordinate” chemistry [46–54]. In 1976, Schleyer and coworkers identified ptC as local minima in lithium-substituted cyclopropane and cyclopropene computationally and marked the beginning of the theoretical [45,55–62] and experimental [63–65] investigations in this area. A lot of attention has been paid to this field recently as a result of the tremendous theoretical and experimental progress made in the pursuit of a stable compound using planar hypercoordinate compounds. The exploration of planar tetracoordinate chemistry has also extended to the hetero atoms and also to the transition metals. In 2003, Frenking and co-workers predicted, theoretically, a novel type of a transition metal-centered aromatic compound in which planar penta-coordinate iron was first introduced [66]. In the same year, Tanaka et al.’s experimental and theoretical studies on Au_5Zn^+ revealed the lowest energy isomer as a planar tetracoordinate Zn, which is stabilized via σ aromaticity [67,68]. Later, in 2004, the same group further identified planar motifs in gold clusters doped with transition metals, including planar tetracoordinate iron [69]. In 2006, Lievens, Nguyen, and co-workers explored the flat structural motifs in $\text{Ag}_5\text{X}^{0/-/+}$ ($\text{X} = \text{Sc}, \text{Ti}, \text{V}, \text{Cr}, \text{Mn}, \text{Fe}, \text{Co}, \text{and Ni}$), where planar tetra and penta-coordinate iron were reported [70,71]. In 2005, Wang and co-workers discovered planar hexacoordinate species in transition metal-doped gold clusters, M@Au_6 ($\text{M} = \text{Ti}, \text{V}, \text{Cr}$) [72]. This research trend was expanded to include other transition metals from Sc to Ni, and planar hexacoordinate molecules were discovered in these gold clusters by Zhang et al. [73]. Planar heptacoordinate Sc was identified as the global minimum in the Cu_7Sc cluster in 2008 by Nguyen and co-workers [74]. Li, Schleyer, and co-workers investigated unconventional planar motifs with hepta-, octa-, nona-, and decacoordinate first-row transition metals enclosed by boron rings with many neutral and charged molecules including planar octa- and nonacoordinate iron as global minima [75,76]. Later, in 2012, Romanescu et al. experimentally reported both the planar octa- and nonacoordinate in FeB_8^- and FeB_9^- clusters [77]. Zhang et al. attempted to design graphene-like materials containing planar hypercoordinate transition metal atoms by constructing FeB_6 monolayers [78]. Zhao and co-workers recently developed a stable FeSi_2 monolayer with planar hexacoordinate Fe atoms [79]. Thimmakonda and co-workers studied the interaction of planar penta-coordinate carbon within a ferrocene derivative [80]. Planar penta-coordinate Zn group elements supported by lithium clusters were found to be global minima by Guha and co-workers [81]. Very recently, planar hexacoordinate transition metals in star structures were identified as global minima [82]. In this direction, the present work aimed to find various geometries of $\text{FeC}_4\text{H}_2^{2+}$ as they are astronomically relevant molecules. Since the four-carbon cumulene carbene, butatrienyliene (C_4H_2), has already been detected in the interstellar medium (ISM) [83], this study explored the species that might potentially mix with transition metals like iron. It is noted here that, in total, eight cumulene carbene molecules of the type C_nH_2 ($n = 3$ to 10) are well-known in the laboratory [84–88], and among them, four lower homologues ($n = 3$ to 6) have already been identified in the ISM [83,89–91]. Despite being the most abundant metal in the universe, iron is less common in the ISM, and hitherto, many have strived to find the missing iron in the interstellar medium [92]. Very recently, for the first time, FeC radical was detected in the envelope of IRC+10216 [93].

In the present work, the isomers of $\text{FeC}_4\text{H}_2^{2+}$ in their singlet, triplet, and quintet electronic states are explored, with an emphasis on planar tetracoordinate iron (ptFe) in the singlet electronic state, and the bonding features of the ptFe structure are also analyzed. This study explores the isomers of $\text{FeC}_4\text{H}_2^{2+}$, where a ptFe is serendipitously identified and is a local minimum. It is noteworthy that iron is in a +2 oxidation state, which is a more commonly occurring oxidation state, and therefore, the $\text{FeC}_4\text{H}_2^{2+}$ system is taken into account here. Iron (II) is integral to various fields of chemistry, including redox reactions, coordination chemistry, and biological systems [94–97]. For brevity, the interaction of counter ions that can neutralize the system was not considered in the current study.

2. Computational Calculation Methodology

The geometries of all isomers of $\text{FeC}_4\text{H}_2^{2+}$ were generated by chemical intuition. Quantum chemical calculations on the singlet electronic state of the system were carried out using the Density Functional Theory (DFT) approach. The possible structures were optimized using the $\omega\text{B97X-D}$ hybrid functional method that uses a version of Grimme's D2 dispersion model. The Restricted Open-Shell Hartree-Fock (ROHF) method was utilized for the triplet and quintet electronic states optimization [98]. The effective core potential (ECP), Stuttgart/Dresden, SDD was used for iron metal, and the large 6-311++G (2d, 2p) basis set for carbon and hydrogen atoms for the investigated system [99–102]. Relativistic effects were significant for molecules containing heavy metals and transition metals; hence, the ECP was considered for the iron system. ECP was used to replace the core with analytical functions that more effectively and precisely represent the combined nuclear-electronic core to the remaining electrons [103]. To confirm whether the stationary point obtained on the potential energy surface (PES) is a minimum or a transition state, or an n th order saddle point, harmonic vibrational frequencies were computed for all the energy-minimized geometries at the same level. All the computational calculations were carried out with the Gaussian suite of programs [104]. Natural bond orbital (NBO) analysis was carried out at the same level of theory. NBO analysis provides information on the charge distribution of the atoms in the molecules and also the Wiberg bond index (WBI) values that are the electronic parameters related to the electron density between atoms. NBO 3.1 implemented in Gaussian 16 was utilized for this purpose [105,106]. Adaptive natural density partitioning (AdNDP) analysis was utilized to further investigate the bonding characteristics [107,108]. A topological analysis of the ptFe isomer was carried out using the Multiwfn program [109,110] with the wavefunction file generated by the Gaussian program [104].

3. Results and Discussions

The potential energy surface (PES) of $\text{FeC}_4\text{H}_2^{2+}$ in the singlet, triplet, and quintet electronic states was explored. The ten energetically low-lying isomers of the singlet electronic state of the $\text{FeC}_4\text{H}_2^{2+}$ system are shown in Figure 1 with their relative energies, point groups, number of imaginary frequencies, and dipole moments. All other optimized isomers of $\text{FeC}_4\text{H}_2^{2+}$ in the singlet electronic state are provided in the Supplementary Material. For brevity, the total electronic energies, zero-point vibrational energy (ZPVE) corrections, ZPVE-corrected total energies (E+ZPVE), absolute dipole moments, relative energies without (ΔE) and with ZPVE corrections ($\Delta E + \text{ZPVE}$), and the number of imaginary frequencies (NImag) are provided in Table S1 in the Supplementary Material. In the unrestricted $U\omega\text{B97X-D}$ approach (results are provided in the Supporting Information), the optimization of the quintet and triplet electronic states shows significant and non-trivial spin contamination. Therefore, we made an effort to optimize the geometries in the triplet and quintet electronic states with the ROHF wavefunction to prevent spin contamination. Nevertheless, in the triplet and quintet electronic states without spin contamination, the number of optimal geometries was lowered to four. The optimized geometries of the triplet and quintet electronic states with ROHF are shown in Figure 2. Isomers **1s**, **1t**, and **1q** are the global minima of the singlet, triplet, and quintet electronic states, respectively. **1s** has

a linear structure, and the structure like iron is directly attached to the cumulene carbene. As cumulene carbene has already been detected in the interstellar medium (ISM) [83], the global minimum of singlet electronic state **1s** suggests that the presence of iron atoms in the ISM might be in the form of these iron hydrogenated carbides. The isovalent pentatetraenyliidene, an isomer of C_5H_2 , has already been a familiar molecule in the laboratory as well as in the ISM [84,90]. As **1s** is a global minimum, it has a higher chance of being viable in the laboratory. It is also polar with a dipole moment value of 1.25 Debye indicating feasible detection in the ISM. **4s** contains planar tetracoordinate iron (ptFe), which should be considered an accidental surprise in the PES of the singlet electronic state. **1t** also contains ptFe, which has been identified as a global minimum in the PES of the triplet electronic state. **1q** has a cyclic structure that is a local minimum in the singlet electronic state, and a similar geometry has been identified as a local minimum (**2t**) in the triplet electronic state. The main focus of the present work was on isomer **4s**, which contains ptFe in the singlet electronic state. It lies ~ 28.15 kcal mol $^{-1}$ above its lowest energy isomer, **1s**. The point group of **4s** is C_{2v} , and its dipole moment value is 1.16 Debye. To probe into the ptFe, the chemical bonding characteristic features were investigated in detail.

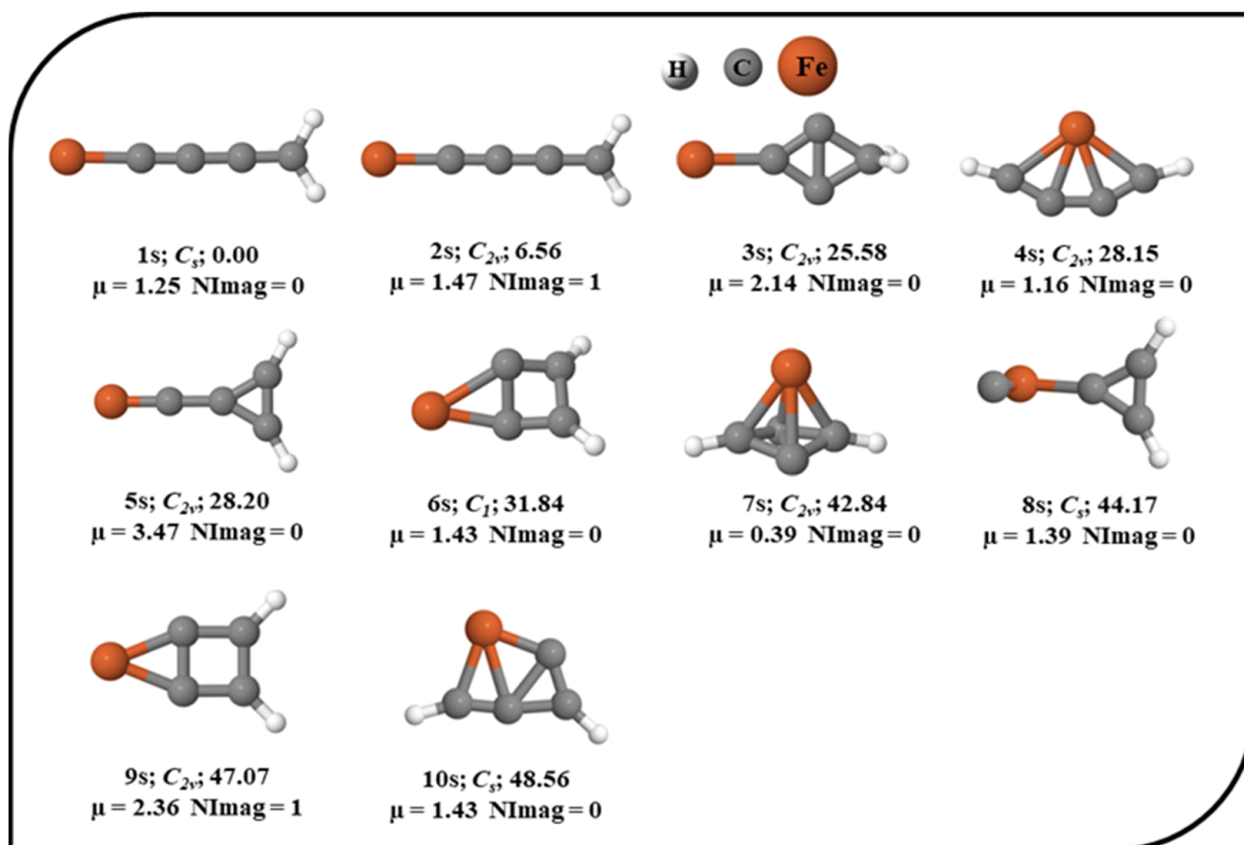


Figure 1. Ten low-lying isomers of $FeC_4H_2^+$ in their corresponding singlet electronic state with the ZPVE-corrected relative energies (in kcal mol $^{-1}$), point groups, dipole moments (in Debye), and the number of imaginary frequencies (NImag) obtained using the ω B97X–D functional with SDD and 6–311++G (2d, 2p) basis sets.

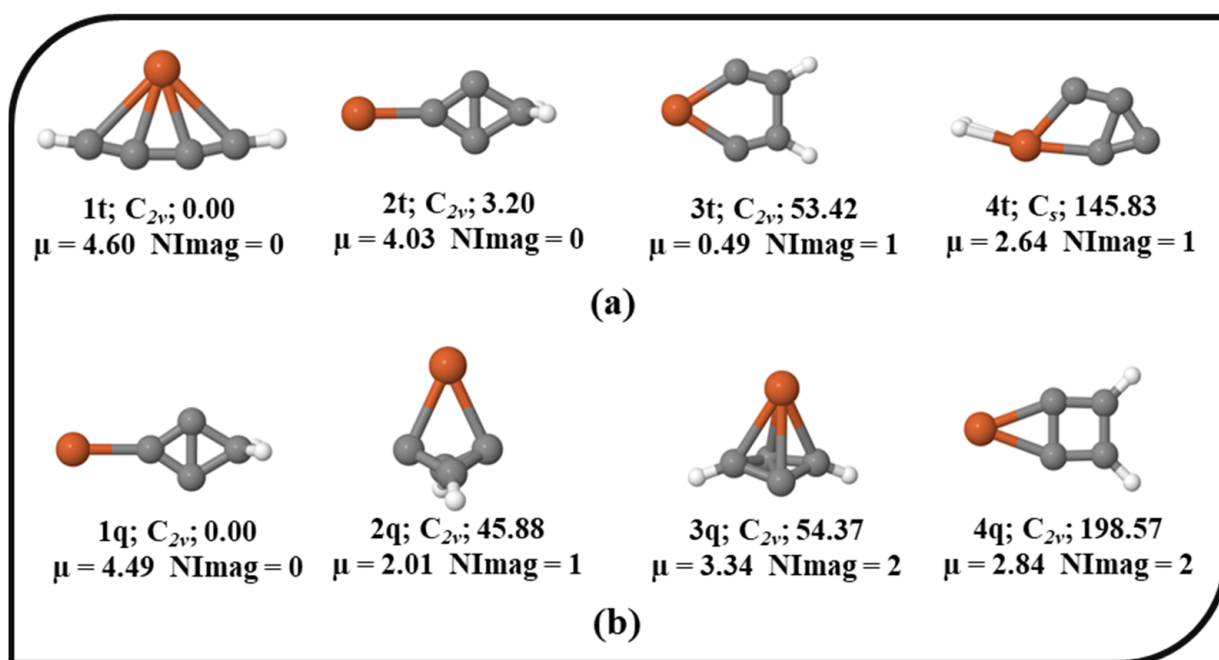


Figure 2. The isomers of $\text{Fe}_4\text{C}_2\text{H}_2^+$ in their corresponding (a) triplet and (b) quintet electronic states with the ZPVE-corrected relative energies (in kcal mol^{-1}), point groups, dipole moments (in Debye), and the number of imaginary frequencies (NImag) obtained using the ROHF method with SDD and 6-311++G (2d, 2p) basis sets.

3.1. Bonding, Wiberg Bond Indices, and Molecular Orbital Analysis

The bonding scenario of 4s exhibiting ptFe was analyzed. The different views, bond lengths, and WBI values of 4s are shown in Figure 3. The Fe–C bond lengths in the ptFe are 2.01 and 2.17 Å, which are in close agreement with the bond lengths already reported in iron–carbon-based molecules [69,71,111–113]. The carbon–carbon bond lengths in 4s are also similar to the reported iron–carbon-based molecules [23,112], and also, it has electron delocalization along the carbon chain. The electronic characteristics associated with the overlap of the electron populations between two atoms are measured using the WBI. Here, the WBI values of ptFe indicate its chemical bonding characteristics. For 4s , the WBI values for C2–Fe and C3–Fe are 0.34, and C1–Fe and C4–Fe are 0.54, indicating the existence of covalent interaction between iron and carbon atoms. These values are in good agreement with the values reported in iron–carbon- and boron-based clusters [75,76]. The carbon–carbon WBI values range from 1.30 to 2.32, reflecting the bonding features arising from the delocalization of electrons. The natural bond orbital (NBO) analysis provides insight into the natural atomic charges (NAC) of the system. The NAC on 4s are depicted in Figure S3 in the Supplementary Material. According to the NAC, the metal center in the ptFe shows a large positive value of 1.257. The NAC on the carbon atoms are low, indicating a large charge transfer between iron and the carbon atoms. The polarity of the system varies because of the differences in electronegativities between carbon and iron. Electrostatic attraction results from this, which makes the ptFe more stable.

To extract more information on bonding, a molecular orbital analysis is carried out. The molecular orbitals of 4s are shown in Figure 4. HOMO, HOMO–2, and HOMO–5 are π delocalization orbitals, whereas HOMO–1, HOMO–3, HOMO–4, and HOMO–6 are σ delocalization orbitals. HOMO–6 clearly shows the covalent interaction between iron and carbon atoms from the overlap of the orbitals. The LUMO to LUMO+6 orbitals are also depicted in Figure 4. The HOMO–LUMO gap is 7.883 eV. Along with σ and π delocalizations, this large energy gap also plays an important role in maintaining the stability of the ptFe.

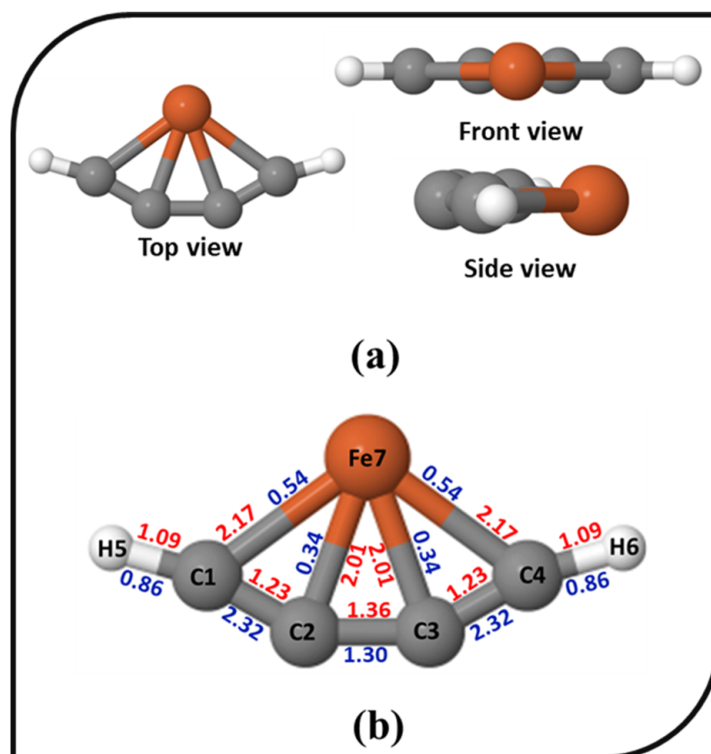


Figure 3. (a) The top, front, and side views of the ptFe, 4s; (b) The bond lengths (in Å, red) and the Wiberg bond indices (in blue) of 4s obtained using the ω B97X-D functional with SDD and 6-311++G (2d, 2p) basis sets.

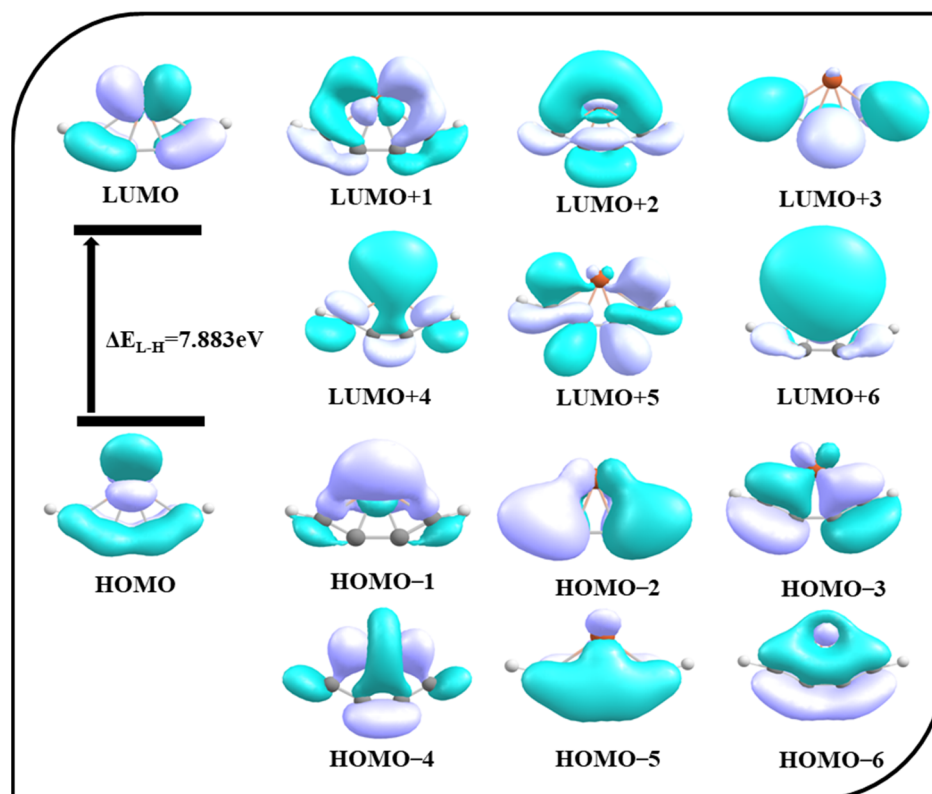


Figure 4. Molecular orbitals of 4s obtained using the ω B97X-D functional with SDD and 6-311++G (2d, 2p) basis sets.

3.2. Adaptive Natural Density Partitioning (AdNDP) Analysis

The AdNDP analysis was employed to comprehend the nature of bonding in the ptFe isomer. This method is an extension of NBO and a powerful approach for the analysis of electron density. The chemical bonding in molecules with non-classical bonding patterns may be described succinctly and simply using this technique. In using this method, the charge density is divided into components with the highest possible degree of localized electron pairs, such as n -center two-electron (n c–2e) bonds, which include core electrons, lone pairs (LPs), and multicentered two-electron bonds like 2c–2e. AdNDP is an excellent implementation to search for delocalized n -center two-electron bonds ($n < 2$) due to the extension of the Lewis description.

The AdNDP bonding patterns of **4s** with occupation numbers (ONs) are depicted in Figure 5. The four 3c–2e σ bonds in **4s** have ON values of 1.99 |e| and 2.00 |e|, which ascertain the electron density localized between the planar tetracoordinate center and their adjacent atoms. The presence of 3c–2e, 4c–2e, and 5c–2e π bonds confirms the presence of alternate delocalized π bonds in the ptFe, which aid in the stabilization of the molecule. The stability of the ptFe is additionally supported by the presence of 5c–2e and 7c–2e σ bonds.

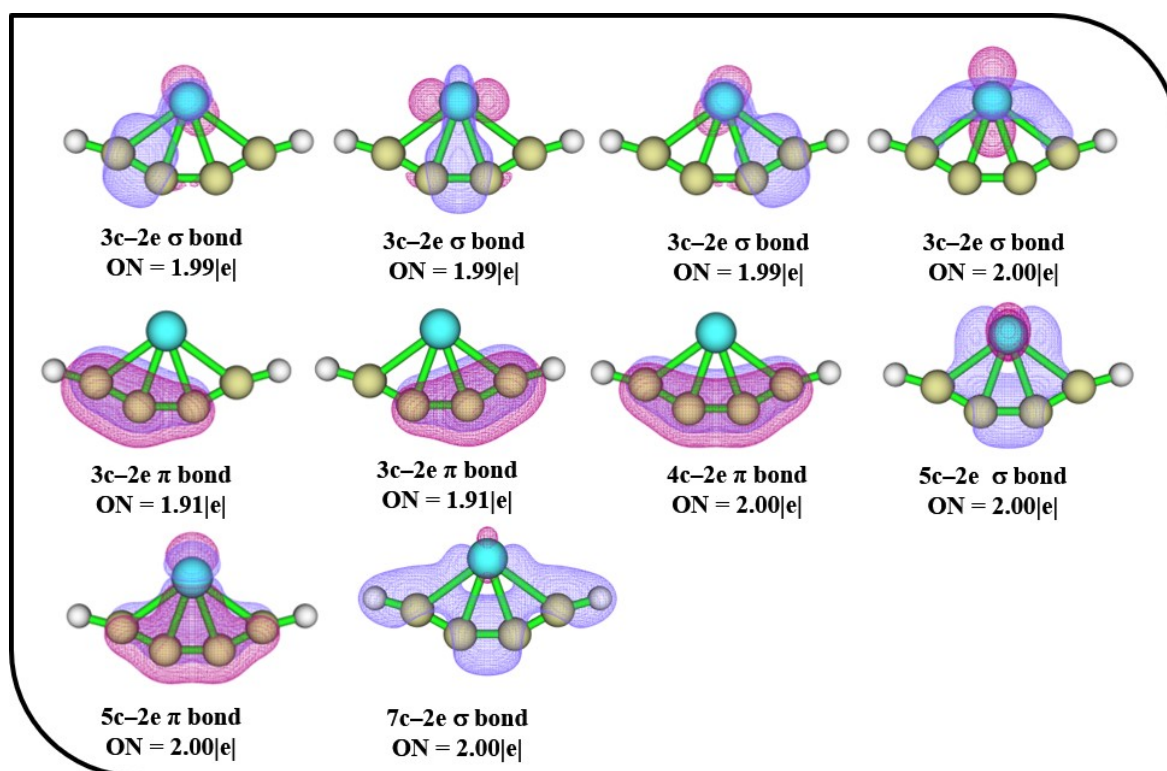


Figure 5. AdNDP bonding patterns of **4s** with occupation numbers (ONs) were obtained using the ω B97X–D functional with SDD and 6–311++G (2d, 2p) basis sets.

3.3. Topological Analysis: Electron Localization Function and Laplacian of Electron Density

A topological analysis was carried out to shed light on the bonding characteristics of ptFe. The electron localization function (ELF) and Laplacian of electron density ($\Delta^2\rho(r)$) were used for the investigation of the topologies of the molecules, which depict the localization of electron pairs and can be used to visualize delocalized bonds. The color-filled map of the ELF and the contour map of the Laplacian of electron density ($\Delta^2\rho(r)$) for **4s** are shown in Figure 6. The interaction between the d-orbitals of iron and adjacent atoms can be observed from the ELF plots. From the contour plot, it is clear that the carbon chain has localized electron density, demonstrating high electron localization that fosters the stability of the ptFe. In **4s**, the electron density for peripheral carbon atoms is higher, resulting in

a higher WBI value of 0.54 when compared to the inner carbon atom, which has a value of 0.34. The plots generated show the interaction between the iron atom and the surrounding carbon atoms and also the delocalization of electron densities within the molecule.

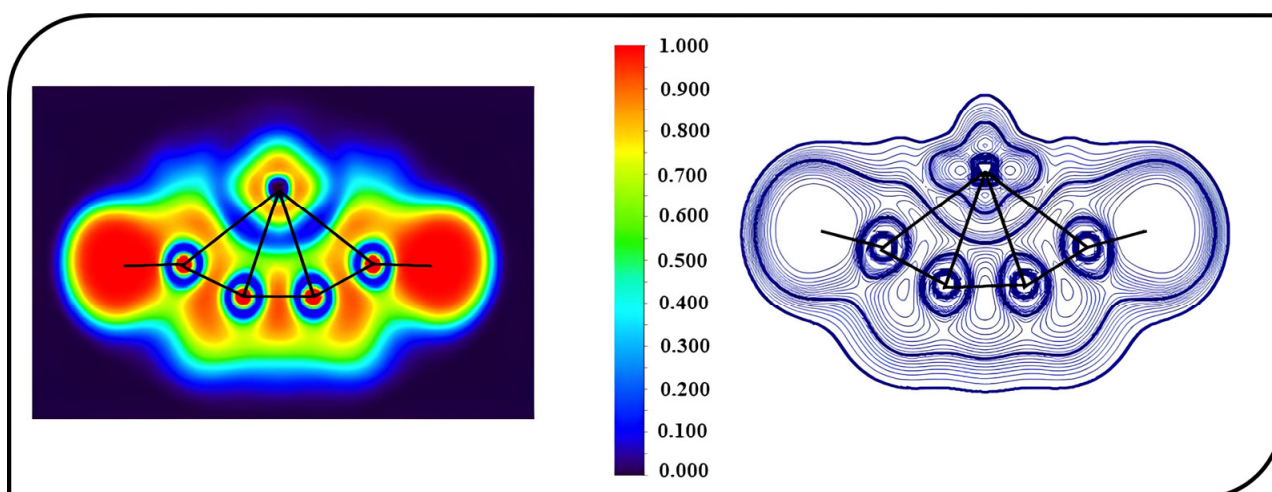


Figure 6. Color-filled map of the ELF and the contour map of the Laplacian of electron density ($\Delta^2\rho(r)$) for **4s** obtained using the ω B97X–D functional with SDD and 6–311++G (2d, 2p) basis sets.

3.4. IR and Raman Spectra

The IR (infrared) and Raman spectra for **4s** computed *in silico* are provided in the Supplementary Material in Figure S4, which assist further experimental observations. The observed vibrational frequencies in the simulated spectra are due to the C=C, Fe–C, and C–H bonds. The absorptions for allenic C=C asymmetric and symmetric stretching occur around 1956 cm^{-1} and 2119 cm^{-1} , respectively. The symmetric and asymmetric stretching of C–H is around 3240 cm^{-1} . The Fe–C asymmetric stretching is at 598 cm^{-1} , whereas in the Raman spectra, the Fe–C mode is observed at 499 cm^{-1} . The IR and Raman spectra were generated with the Gaussian program [101]. The computationally predicted IR and Raman spectra would be useful for the detection of the **4s** structure in the experimental laboratory.

4. Conclusions

The isomers of the $\text{FeC}_4\text{H}_2^{2+}$ system in the singlet electronic state were investigated first with the DFT method, whereas triplet and quintet electronic states were explored using the ROHF method. Planar tetracoordinate iron (ptFe) was found on the PES while exploring the isomers of the $\text{FeC}_4\text{H}_2^{2+}$ system. A thorough bonding analysis was performed on the **4s** ptFe isomer. Different methods such as the AdNDP, WBI, NBO, and ELF were used to obtain insight into the structural characteristics. The delocalized bonds that stabilize the ptFe in the singlet electronic state are well supported by the AdNDP, NBO, and WBI. The WBI values in **4s** indicate the covalent characteristics of the Fe–C bond in the ptFe. The electron density around carbon and iron in the color-filled ELF plot depicts the stability of the ptFe. The topological analysis through the ELF and the Laplacian of electron density ($\Delta^2\rho(r)$) confirms the interaction between ptFe and the carbon atoms surrounding them. The stable nature of the ptFe is also attained through favorable molecular orbital interactions. The computed IR and Raman spectra of the ptFe could be useful for experimentalists for identification in the laboratory in the future. The results of the present work provide new directions to theoretical and experimental studies on flat transition metal–carbon hydride chemistry.

Supplementary Materials: The following supporting information can be downloaded at <https://www.mdpi.com/article/10.3390/atoms12020011/s1>. The optimized geometries of $\text{FeC}_4\text{H}_2^{2+}$ in the singlet electronic state are shown in Figure S1; the AdNDP bonding patterns of 4s in the singlet electronic state with occupation numbers (ON) are shown in Figure S2; NBO charges (in $|e|$) on 4s obtained using the $\omega\text{B97X-D}$ functional with SDD and 6-311++G (2d, 2p) basis sets are shown in Figure S3; the IR vibrational spectrum and Raman spectrum of 4s obtained using the $\omega\text{B97X-D}$ functional with SDD and 6-311++G (2d, 2p) basis sets are shown in Figure S4; the isomers of $\text{FeC}_4\text{H}_2^{2+}$ in the triplet and quintet electronic states with ZPVE-corrected relative energies (in kcal mol^{-1}), dipole moments (in Debye), and the number of imaginary frequencies (NImag) obtained using the (U) $\omega\text{B97X-D}$ functional with SDD and 6-311++G (2d, 2p) basis sets in Figures S5 and S6, respectively, total energy (in a.u.), zero-point correction (in a.u.), ZPVE-corrected total energy (E+ZPVE; in a.u.), relative energy ($\Delta E + \text{ZPVE}$; in kcal mol^{-1}), dipole moment (in Debye), and the number of imaginary frequencies (NImag) of $\text{FeC}_4\text{H}_2^{2+}$ in the singlet electronic state calculated at the $\omega\text{B97X-D}$ functional with SDD and 6-311++G (2d, 2p) basis sets are listed in Table S1, and triplet and quintet electronic states calculated using ROHF with SDD and 6-311++G (2d, 2p) basis sets are listed in Tables S2 and S3, respectively; the Cartesian coordinates of all the isomers of $\text{FeC}_4\text{H}_2^{2+}$ in the singlet, triplet, and quintet electronic states are listed in Tables S4, S5, and S6, respectively; and the total energy (in a.u.), point group, zero-point correction (in a.u.), ZPVE-corrected total energy (E + ZPVE; in a.u.), relative energy ($\Delta E + \text{ZPVE}$; in kcal mol^{-1}), dipole moment (in Debye), the number of imaginary frequencies (NImag), the expectation value of the total spin, $\langle S^2 \rangle$, and calculated %error for the spin contamination of $\text{FeC}_4\text{H}_2^{2+}$ in their corresponding triplet and quintet electronic states calculated using (U) $\omega\text{B97X-D}$ functional with SDD and 6-311++G (2d, 2p) basis sets are listed in Tables S7 and S8, respectively.

Author Contributions: Conceptualization, V.S.T., V.C. and K.T. (Krishnan Thirumoorthy); Investigation, S.S., V.S.T., V.C., K.T. (Kandasamy Thirunavukkarsu) and K.T. (Krishnan Thirumoorthy); Methodology, S.S., V.S.T., V.C., K.T. (Kandasamy Thirunavukkarsu) and K.T. (Krishnan Thirumoorthy); Supervision, V.S.T., V.C., K.T. (Kandasamy Thirunavukkarsu) and K.T. (Krishnan Thirumoorthy); Visualization, S.S. and K.T. (Krishnan Thirumoorthy); Writing—Original Draft, S.S.; Writing—Review and Editing, V.S.T., V.C. and K.T. (Krishnan Thirumoorthy). All authors have read and agreed to the published version of the manuscript.

Funding: This research received no external funding.

Institutional Review Board Statement: Not applicable.

Informed Consent Statement: Not applicable.

Data Availability Statement: Data are available in the article or Supplementary Materials.

Acknowledgments: The computational facility provided at the VIT, Vellore, to carry out this work is gratefully acknowledged.

Conflicts of Interest: The authors declare no conflicts of interest.

References

1. Miralrio, A.; Hernández-Hernández, A.; Pescador-Rojas, J.A.; Sansores, E.; López-Pérez, P.A.; Martínez-Farías, F.; Cortes, E.R. Theoretical Study of the Stability and Properties of Magic Numbers ($m = 5$, $n = 2$) and ($m = 6$, $n = 3$) of Bimetallic Bismuth-Copper Nanoclusters; Bi_mCu_n . *Int. J. Quantum Chem.* **2017**, *117*, e25449. [CrossRef]
2. Billas, I.M.L.; De Heer, W.A.; Chatelain, A. Magnetic Properties of Small Iron Systems: From Ferromagnetic Resonance of Precipitated Particles in Silica to Stern-Gerlach Deflections in Molecular Beam. *J. Non Cryst. Solids* **1994**, *179*, 316–323. [CrossRef]
3. Castro, M. The role of the Jahn-teller distortions on the structural, binding, and magnetic properties of small Fe n clusters, $n \leq 7$. *Int. J. Quantum Chem.* **1997**, *64*, 223–230. [CrossRef]
4. Fehner, T.; Halet, J.F.; Saillard, J.Y. *Molecular Clusters: A Bridge to Solid-State Chemistry*; Cambridge University Press: Cambridge, UK, 2007.
5. Li, H.-F.; Li, Z.-Y.; Liu, Q.-Y.; Li, X.-N.; Zhao, Y.-X.; He, S.-G. Methane Activation by Iron-Carbide Cluster Anions FeC_6^- . *J. Phys. Chem. Lett.* **2015**, *6*, 2287–2291. [CrossRef] [PubMed]
6. Allen, M.D.; Pesch, T.C.; Ziurys, L.M. The pure rotational spectrum of FeC ($X^3\Delta_1$). *Astrophys. J.* **1996**, *472*, L57. [CrossRef]
7. Chu, C.J.; Kafafi, Z.H.; Margrave, J.L.; Hauge, R.H.; Billups, W.E. Matrix-Isolation Studies of the Reactions of Ground- and Excited-State Atomic Iron with Cyclopropane. *Organometallics* **2000**, *19*, 39–48. [CrossRef]
8. Balfour, W.J.; Cao, J.; Prasad, C.V.V.; Qian, C.X.W. Electronic Spectroscopy of Jet-Cooled Iron Monocarbide. The $^3\Delta_1 \leftarrow ^3\Delta_1$ Transition near 493 nm. *J. Chem Phys.* **1995**, *103*, 4046–4051. [CrossRef]

9. Tzeli, D.; Mavridis, A. Accurate Ab Initio Calculations of the Ground States of FeC, FeC⁺, and FeC⁻. *J. Chem. Phys.* **2010**, *132*, 194312. [[CrossRef](#)]
10. Tzeli, D.; Mavridis, A. Theoretical Investigation of Iron Carbide, FeC. *J. Chem. Phys.* **2002**, *116*, 4901–4921. [[CrossRef](#)]
11. Li, C.G.; Zhang, J.; Zhang, W.Q.; Tang, Y.N.; Ren, B.Z.; Hu, Y.F. First-Principle Study of Structural, Electronic and Magnetic Properties of (FeC)_n (n = 1–8) and (FeC)₈TM (TM = V, Cr, Mn and Co) Clusters. *Sci. Rep.* **2017**, *7*, 17516. [[CrossRef](#)]
12. Steglich, M.; Chen, X.; Johnson, A.; Maier, J.P. UV Spectra of Iron-Doped Carbon Clusters FeC_n n = 3–6. *Int. J. Mass Spectrom.* **2014**, *365–366*, 351–355. [[CrossRef](#)]
13. Huysken, F.; Kohn, B.; Alexandrescu, R.; Morjan, I. Reactions of Iron Clusters with Oxygen and Ethylene: Observation of Particularly Stable Species. *J. Chem. Phys.* **2000**, *113*, 6579–6584. [[CrossRef](#)]
14. Ball, D.W.; Pong, R.G.S.; Kafafi, Z.H. Reactions of Atomic and Diatomic Iron with Allene in Solid Argon. *J. Am. Chem. Soc.* **1993**, *115*, 2864–2870. [[CrossRef](#)]
15. Glukhovtsev, M.N.; Bach, R.D.; Nagel, C.J. Performance of the B3LYP/ECP DFT Calculations of Iron-Containing Compounds. *J. Phys. Chem. A* **1997**, *101*, 316–323. [[CrossRef](#)]
16. Pilgrim, J.S.; Duncan, M.A. Metallo-Carbohedrenes: Chromium, Iron, and Molybdenum Analogs. *J. Am. Chem. Soc.* **1993**, *115*, 6958–6961. [[CrossRef](#)]
17. Nash, B.K.; Rao, B.K.; Jena, P. Equilibrium Structure and Bonding of Small Iron-Carbon Clusters. *J. Chem. Phys.* **1996**, *105*, 11020–11023. [[CrossRef](#)]
18. Noya, E.G.; Longo, R.C.; Gallego, L.J. Geometric Structure and Electronic Properties of Neutral and Anionic Fe₂C₃ and Fe₂C₄ Clusters, as Obtained by Density-Functional Calculations. *J. Chem. Phys.* **2004**, *120*, 2069–2070. [[CrossRef](#)]
19. Noya, E.G.; Longo, R.C.; Gallego, L.J. Density-Functional Calculations of the Structures, Binding Energies, and Spin Multiplicities of Fe-C Clusters. *J. Chem. Phys.* **2003**, *119*, 11130–11134. [[CrossRef](#)]
20. Largo, L.; Barrientos, C.; Redondo, P. Small Iron Doped Carbon Clusters: A Comparison with Early and Late First-Row Transition Metal Doped Clusters. *J. Chem. Phys.* **2009**, *130*, 134304. [[CrossRef](#)]
21. Zhang, B.; Cao, B.B.; Chen, C.; Zhang, J.; Duan, H.M. Density-Functional Theory Study on Neutral and Charged MnC₂ (M = Fe, Co, Ni, Cu; n = 1–5) Clusters. *J. Clust. Sci.* **2013**, *24*, 197–207. [[CrossRef](#)]
22. Limon, P.; Miralrio, A.; Castro, M. Characterization of Magnetic Series of Iron-Carbon Clusters FeNC₀, ±1 (n ≤ 13). *J. Phys. Chem. C* **2020**, *124*, 9484–9495. [[CrossRef](#)]
23. Zhang, Z.X.; Cao, B.B.; Duan, H.M. Density-Functional Calculations of MnC (M = Fe, Co, Ni, Cu, n = 1–6) Clusters. *J. Mol. Struct. Theochem* **2008**, *863*, 22–27. [[CrossRef](#)]
24. Wang, L.-S.; Li, X. Vibrationally Resolved Photoelectron Spectroscopy of the First Row Transition Metal and C₃ Clusters: MC₃⁻ (M=Sc, V, Cr, Mn, Fe, Co, and Ni). *J. Chem. Phys.* **2000**, *112*, 3602–3608. [[CrossRef](#)]
25. Lebrilla, C.B.; Drewello, T.; Schwarz, H. Formation and Detection of Neutral FeCH_x (x = 0–3) Using Neutralization-Reionization Mass Spectrometry (NRMS). *Organometallics*. **1987**, *6*, 2268–2270. [[CrossRef](#)]
26. Fan, J.; Wang, L.-S. A Study of FeC₂ and FeC₂H by Anion Photoelectron Spectroscopy. *J. Phys. Chem.* **1994**, *98*, 11814–11817. [[CrossRef](#)]
27. Husband, J.; Aguirre, F.; Thompson, C.J.; Laperle, C.M.; Metz, R.B. Photofragment Spectroscopy of FeCH₂⁺, CoCH₂⁺, and NiCH₂⁺ near the M⁺-CH₂ Dissociation Threshold. *J. Phys. Chem. A* **2000**, *104*, 2020–2024. [[CrossRef](#)]
28. Drechsler, G.; Boesl, U. Mass Selective Photodetachment Photoelectron Spectroscopy: Small Transition Metal (Fe, Ni) Carbon Hydrogen Compounds. *Int. J. Mass Spectrom.* **2003**, *228*, 1067–1082. [[CrossRef](#)]
29. Chang, C.; Patzer, A.B.C.; Kegel, W.H.; Chandra, S. Small Fe Bearing Ring Molecules of Possible Astrophysical Interest: Molecular Properties and Rotational Spectra. *Astrophys. Space Sci.* **2013**, *347*, 315–325. [[CrossRef](#)]
30. Guo, B.C.; Kerns, K.P.; Castleman, A.W., Jr. Ti₈C¹²⁺-metallo-carbohedrenes: A New Class of Molecular Clusters? *Science* **1992**, *255*, 1411–1413. [[CrossRef](#)]
31. Ryzhkov, M.V.; Delley, B. Geometry, electronic structure, and magnetic ordering of iron-carbon nanoparticles. *Theor. Chem. Acc.* **2012**, *131*, 1144. [[CrossRef](#)]
32. Ryzhkov, M.V.; Ivanovskii, A.L.; Delley, B.T. Electronic Structure and Geometry Optimization of Nanoparticles Fe₂C, FeC₂, Fe₃C, FeC₃ and Fe₂C₂. *Chem Phys Lett.* **2005**, *404*, 400–408. [[CrossRef](#)]
33. Hensley, B.S.; Draine, B.T. Thermodynamics and charging of interstellar iron nanoparticles. *Astrophys. J.* **2017**, *834*, 134. [[CrossRef](#)]
34. Rohmer, M.M.; Bénard, M.; Poblet, J.-M. Structure, Reactivity, and Growth Pathways of Metallo-carbohedrenes M₈C₁₂ and Transition Metal/Carbon Clusters and Nanocrystals: A Challenge to Computational Chemistry. *Chem. Rev.* **2000**, *100*, 495–542. [[CrossRef](#)]
35. Geng, C.; Li, J.; Weiske, T.; Schwarz, H. A Reaction-Induced Localization of Spin Density Enables Thermal C–H Bond Activation of Methane by Pristine FeC⁴⁺. *Chem. A Eur. J.* **2019**, *25*, 12940–12945. [[CrossRef](#)]
36. Hu, Y.; Jensen, J.O.; Zhang, W.; Cleemann, L.N.; Xing, W.; Bjerrum, N.J.; Li, Q. Hollow Spheres of Iron Carbide Nanoparticles Encased in Graphitic Layers as Oxygen Reduction Catalysts. *Angew. Chem. Int. Ed.* **2014**, *53*, 3675–3679. [[CrossRef](#)]
37. Li, S.; Yang, J.; Song, C.; Zhu, Q.; Xiao, D.; Ma, D. Iron Carbides: Control Synthesis and Catalytic Applications in CO_x Hydrogenation and Electrochemical HER. *Adv. Mater.* **2019**, *31*, e1901796. [[CrossRef](#)]
38. Wang, X.; Zhu, K.; Ju, Y.; Li, Y.; Li, W.; Xu, J.; Hou, Y. Iron Carbides: Magic Materials with Magnetic and Catalytic Properties. *J. Magn. Magn. Mater.* **2019**, *489*, 165432. [[CrossRef](#)]

39. Li, Y.; Li, Z.; Ahsen, A.; Lammich, L.; Mannie, G.J.A.; Niemantsverdriet, J.W.H.; Lauritsen, J.V. Atomically Defined Iron Carbide Surface for Fischer-Tropsch Synthesis Catalysis. *ACS Catal.* **2019**, *9*, 1264–1273. [[CrossRef](#)]
40. Miyaoka, H.; Ichikawa, T.; Fujii, T.; Ishida, W.; Isobe, S.; Fuji, H.; Kojima, Y. Anomalous Hydrogen Absorption on Non-Stoichiometric Iron-Carbon Compound. *J. Alloys Compd.* **2010**, *507*, 547–550. [[CrossRef](#)]
41. Wu, X.; Dong, J.; Qiu, M.; Li, Y.; Zhang, Y.; Zhang, H.; Zhang, J. Subnanometer Iron Clusters Confined in a Porous Carbon Matrix for Highly Efficient Zinc-Air Batteries. *Nanoscale Horiz.* **2020**, *5*, 359–365. [[CrossRef](#)]
42. Fan, D.; Chen, C.; Lu, S.; Li, X.; Jiang, M.; Hu, X. Highly Stable Two-Dimensional Iron Monocarbide with Planar Hypercoordinate Moiety and Superior Li-Ion Storage Performance. *ACS Appl. Mater. Interfaces.* **2020**, *12*, 30297–30303. [[CrossRef](#)]
43. Xiang, T.; Chen, Z.; Rao, Z.; Yan, M.; Feng, Z.; Li, X.; Yang, H.; Huang, J.; Shen, X. Hierarchical Fe/Fe₃C/C Nanofibers as Anodes for High Capacity and Rate in Lithium Ion Batteries. *Ionics* **2021**, *27*, 3663–3669. [[CrossRef](#)]
44. Monkhorst, H.J. Activation Energy for Interconversion of Enantiomers Containing an Asymmetric Carbon Atom without Breaking Bonds. *Chem. Commun.* **1968**, *18*, 1111–1112. [[CrossRef](#)]
45. Erker, G. Planar-Tetracoordinate Carbon: Making Stable Anti-van't Hoff/LeBel Compounds. *Comments Inorg. Chem.* **1992**, *13*, 111–131. [[CrossRef](#)]
46. Hoffmann, R.; Alder, R.W.; Wilcox, C.F., Jr. Planar tetracoordinate carbon. *J. Am. Chem. Soc.* **1970**, *92*, 4992–4993. [[CrossRef](#)]
47. Ravell, E.; Jalife, S.; Barroso, J.; Orozco-Ic, M.; Hernández-Juárez, G.; Ortiz-Chi, F.; Pan, S.; Cabellos, J.L.; Merino, G. Structure and Bonding in CE₅[−] (E=Al-Tl) Clusters: Planar Tetracoordinate Carbon versus Pentacoordinate Carbon. *Chem. Asian J.* **2018**, *13*, 1467–1473. [[CrossRef](#)]
48. Sarkar, P.; Thirumorthy, K.; Anoop, A.; Thimmakonda, V.S. Planar Pentacoordinate Carbon in [XC₇H₂]₂⁺ (X = Be and Mg) and Its Derivatives. *Phys. Chem. Chem. Phys.* **2022**, *24*, 27606–27611. [[CrossRef](#)]
49. Leyva-Parra, L.; Diego, L.; Yañez, O.; Inostroza, D.; Barroso, J.; Vásquez-Espinal, A.; Merino, G.; Tiznado, W. Planar Hexacoordinate Carbons: Half Covalent, Half Ionic. *Angew. Chem. Int. Ed.* **2021**, *60*, 8700–8704. [[CrossRef](#)]
50. Jimenez-Halla, J.O.C.; Wu, Y.-B.; Wang, Z.-X.; Islas, R.; Heine, T.; Merino, G. CA14Be and CA13Be₂: Global Minima with a Planar Pentacoordinate Carbon Atom. *Chem. Commun.* **2010**, *46*, 8776–8778. [[CrossRef](#)] [[PubMed](#)]
51. Yañez, O.; Báez-Grez, R.; Garza, J.; Pan, S.; Barroso, J.; Vásquez-Espinal, A.; Merino, G.; Tiznado, W. Embedding a Planar Hypercoordinate Carbon Atom into a [4n+2] π-System. *ChemPhysChem* **2020**, *21*, 145–148. [[CrossRef](#)]
52. Wang, L.-M.; Huang, W.; Averkiev, B.B.; Boldyrev, A.I.; Wang, L.-S. CB₇[−]: Experimental and Theoretical Evidence against Hypercoordinate Planar Carbon. *Angew. Chem. Int. Ed.* **2007**, *46*, 4550–4553. [[CrossRef](#)]
53. Malhan, A.H.; Thimmakonda, V.S.; Thirumorthy, K. Five Bonds to Carbon through Tri-Coordination in Al₃C₃^{−/0}. *Chemistry* **2023**, *5*, 1113–1123. [[CrossRef](#)]
54. Malhan, A.H.; Thirumorthy, K. Global minimum and a heap of low-lying isomers with planar tetracoordinate carbon in CA13MgH₂-system. *Phys. Chem. Chem. Phys.* **2024**, *26*, 3804–3809. [[CrossRef](#)]
55. Cui, Z.-H.; Contreras, M.; Ding, Y.-H.; Merino, G. Planar Tetracoordinate Carbon versus Planar Tetracoordinate Boron: The Case of CB₄ and Its Cation. *J. Am. Chem. Soc.* **2011**, *133*, 13228–13231. [[CrossRef](#)] [[PubMed](#)]
56. Collins, J.B.; Dill, J.D.; Jemmis, E.D.; Apeloig, Y.; Schleyer, P.V.R.; Seeger, R.; Pople, J.A. Stabilization of planar tetracoordinate carbon. *J. Am. Chem. Soc.* **1976**, *98*, 5419–5427. [[CrossRef](#)]
57. Thimmakonda, V.S.; Thirumorthy, K. Si₃C₂H₂ Isomers with a Planar Tetracoordinate Carbon or Silicon Atom(s). *Comput. Theor. Chem.* **2019**, *1157*, 40–46. [[CrossRef](#)]
58. Das, P.; Khatun, M.; Anoop, A.; Chattaraj, P.K. CSi_nGe_{4−n}²⁺ (n = 1–3): Prospective Systems Containing Planar Tetracoordinate Carbon (ptC). *Phys. Chem. Chem. Phys.* **2022**, *24*, 16701–16711. [[CrossRef](#)]
59. Bai, L.-X.; Barroso, J.; Orozco-Ic, M.; Ortiz-Chi, F.; Guo, J.-C.; Merino, G. CA11[−]: A Molecular Rotor with a Quasi-Planar Tetracoordinate Carbon. *Chem. Commun.* **2023**, *59*, 4966–4969. [[CrossRef](#)]
60. Malhan, A.H.; Sobinson, S.; Job, N.; Shajan, S.; Mohanty, S.P.; Thimmakonda, V.S.; Thirumorthy, K. Al₂C₄H₂ Isomers with the Planar Tetracoordinate Carbon (PtC)/Aluminum (PtAl). *Atoms* **2022**, *10*, 112. [[CrossRef](#)]
61. Job, N.; Khatun, M.; Thirumorthy, K.; Sasanka Sankhar Reddy, C.H.; Chandrasekaran, V.; Anoop, A.; Thimmakonda, V.S. Ca14mg0[−]: Global Minima with a Planar Tetracoordinate Carbon Atom. *Atoms* **2021**, *9*, 24. [[CrossRef](#)]
62. Thirumorthy, K.; Chandrasekaran, V.; Cooksy, A.L.; Thimmakonda, V.S. Kinetic Stability of Si₂C₅H₂ Isomer with a Planar Tetracoordinate Carbon Atom. *Chemistry* **2020**, *3*, 13–27. [[CrossRef](#)]
63. Xu, J.; Zhang, X.; Yu, S.; Ding, Y.-H.; Bowen, K.H. Identifying the Hydrogenated Planar Tetracoordinate Carbon: A Combined Experimental and Theoretical Study of CA1₄H and CA1₄H[−]. *J. Phys. Chem. Lett.* **2017**, *8*, 2263–2267. [[CrossRef](#)] [[PubMed](#)]
64. Ebner, F.; Greb, L. Calix[4]Pyrrole Hydridosilicate: The Elusive Planar Tetracoordinate Silicon Imparts Striking Stability to Its Anionic Silicon Hydride. *J. Am. Chem. Soc.* **2018**, *140*, 17409–17412. [[CrossRef](#)] [[PubMed](#)]
65. Li, X.; Wang, L.-S.; Boldyrev, A.I.; Simons, J. Tetracoordinated Planar Carbon in the Al₄C[−] Anion. A Combined Photoelectron Spectroscopy and Ab Initio Study. *J. Am. Chem. Soc.* **1999**, *121*, 6033–6038. [[CrossRef](#)]
66. Lein, M.; Frunzke, J.; Frenking, G. A Novel Class of Aromatic Compounds: Metal-Centered Planar Cations [Fe(Sb₅)]⁺ and [Fe(Bi₅)]⁺. *Angew. Chem. Int. Ed.* **2003**, *42*, 1303–1306. [[CrossRef](#)]
67. Tanaka, H.; Neukermans, S.; Janssens, E.; Silverans, R.E.; Lievens, P. σ Aromaticity of the Bimetallic Au₅Zn⁺ Cluster. *J. Am. Chem. Soc.* **2003**, *125*, 2862–2863. [[CrossRef](#)]

68. Neukermans, S.; Janssens, E.; Tanaka, H.; Silverans, R.E.; Lievens, P. Element- and Size-Dependent Electron Delocalization in Au_NX^+ Clusters ($X = Sc, Ti, V, Cr, Mn, Fe, Co, Ni$). *Phys. Rev. Lett.* **2003**, *90*, 033401. [CrossRef]
69. Janssens, E.; Tanaka, H.; Neukermans, S.; Silverans, R.E.; Lievens, P. Electron Delocalization in $AuNXM$ ($X=Sc, Ti, Cr, Fe$) Clusters: A Density Functional Theory and Photofragmentation Study. *Phys. Rev. B* **2004**, *69*, 085402. [CrossRef]
70. Hou, X.-J.; Janssens, E.; Lievens, P.; Nguyen, M.T. Theoretical Study of the Geometric and Electronic Structure of Neutral and Anionic Doped Silver Clusters, Ag_5X^{0-} with $X = Sc, Ti, V, Cr, Mn, Fe, Co$, and Ni . *J. Chem. Phys.* **2006**, *330*, 365–379. [CrossRef]
71. Janssens, E.; Hou, X.J.; Nguyen, M.T.; Lievens, P. The Geometric, Electronic, and Magnetic Properties of $Ag_5X + (X=Sc, Ti, V, Cr, Mn, Fe, Co, \text{ and } Ni)$ Clusters. *J. Chem. Phys.* **2006**, *124*, 184319. [CrossRef]
72. Li, X.; Kiran, B.; Cui, L.-F.; Wang, L.-S. Magnetic Properties in Transition-Metal-Doped Gold Clusters: $M@Au_6$ ($M = Ti, V, Cr$). *Phys. Rev. Lett.* **2005**, *95*, 253401. [CrossRef]
73. Zhang, M.; He, L.-M.; Zhao, L.-X.; Feng, X.-J.; Luo, Y.-H. Tuning Magnetic Moments by 3d Transition-Metal-Doped Au_6 Clusters. *J. Phys. Chem. C* **2009**, *113*, 6491–6496. [CrossRef]
74. Hölzl, T.; Janssens, E.; Veldeman, N.; Veszprémi, T.; Lievens, P.; Nguyen, M.T. The Cu_7Sc Cluster Is a Stable σ -Aromatic Seven-Membered Ring. *ChemPhysChem*. **2008**, *9*, 833–838. [CrossRef]
75. Pu, Z.; Ito, K.; Schleyer, P.V.R.; Li, Q.-S. Planar Hepta-, Octa-, Nona-, and Decacoordinate First Row d-Block Metals Enclosed by Boron Rings. *Inorg. Chem.* **2009**, *48*, 10679–10686. [CrossRef] [PubMed]
76. Ito, K.; Pu, Z.; Li, Q.-S.; Schleyer, P.V.R. Cyclic Boron Clusters Enclosing Planar Hypercoordinate Cobalt, Iron, and Nickel. *Inorg. Chem.* **2008**, *47*, 10906–10910. [CrossRef]
77. Romanescu, C.; Galeev, T.R.; Sergeeva, A.P.; Li, W.-L.; Wang, L.-S.; Boldyrev, A.I. Experimental and Computational Evidence of Octa- and Nona-Coordinated Planar Iron-Doped Boron Clusters: $Fe@B_8$ - and $Fe@B_9$ -. *J. Organomet. Chem.* **2012**, *721–722*, 148–154. [CrossRef]
78. Zhang, H.; Li, Y.; Hou, J.; Tu, K.; Chen, Z. FeB_6 Monolayers: The Graphene-like Material with Hypercoordinate Transition Metal. *J. Am. Chem. Soc.* **2016**, *138*, 5644–5651. [CrossRef]
79. Zhao, Y.; Liu, Q.; Xing, J.; Jiang, X.; Zhao, J. $FeSi_2$: A Two-Dimensional Ferromagnet Containing Planar Hexacoordinate Fe Atoms. *Nanoscale Adv.* **2022**, *4*, 600–607. [CrossRef] [PubMed]
80. Shajan, S.; Guo, J.-C.; Sinjari, A.; Thirumoorthy, K.; Thimmakonda, V.S. Pentacoordinate Carbon Atoms in a Ferrocene Dication Derivative— $[Fe(Si_2-\eta^5-C_5H_2)_2]^{2+}$. *Chemistry* **2022**, *4*, 1092–1100. [CrossRef]
81. Kalita, A.J.; Baruah, I.; Sarmah, K.; Borah, R.R.; Yashmin, F.; Guha, A.K. Planar Pentacoordinate Zinc Group Elements Stabilized by Multicentric Bonds. *Inorg. Chem.* **2022**, *61*, 1259–1263. [CrossRef]
82. Bai, L.-X.; Guo, J.-C. σ -Aromatic MA_6S_6 ($M = Ni, Pd, Pt$) Stars Containing Planar Hexacoordinate Transition Metals. *Molecules* **2023**, *28*, 942. [CrossRef]
83. Killian, T.C.; Gottlieb, C.A.; Gottlieb, E.W.; Vrtilik, J.M.; Thaddeus, P. Laboratory Detection of a Second Carbon Chain Carbene—Butatrienylidene, H_2CCCC . *Astrophys. J.* **1990**, *365*, L89–L92. [CrossRef]
84. McCarthy, M.C.; Travers, M.J.; Kovács, A.; Chen, W.; Novick, S.E.; Gottlieb, C.A.; Thaddeus, P. Detection and characterization of the cumulene carbenes H_2C_5 and H_2C_6 . *Science* **1997**, *275*, 518–520. [CrossRef]
85. McCarthy, M.C.; Travers, M.J.; Kovács, A.; Gottlieb, C.A.; Thaddeus, P. Eight new carbon chain molecules. *Astrophys. J. Suppl. Ser.* **1997**, *113*, 105. [CrossRef]
86. Maier, G.; Reisenauer, H.P.; Schwab, W.; Carsky, P.; Hess, B.A., Jr.; Schaad, L.J. Vinylidene carbene: A new C_3H_2 species. *J. Am. Chem. Soc.* **1987**, *109*, 5183–5188. [CrossRef]
87. McCarthy, M.C.; Travers, M.J.; Gottlieb, C.A.; Thaddeus, P. Laboratory detection of the ring-chain molecule C_7H_2 . *Astrophys. J.* **1997**, *483*, L139. [CrossRef]
88. Apponi, A.J.; McCarthy, M.C.; Gottlieb, C.A.; Thaddeus, P. Laboratory detection of four new cumulene carbenes: H_2C_7 , H_2C_8 , H_2C_9 , and D_2C_{10} . *Astrophys. J.* **2000**, *530*, 357. [CrossRef]
89. Kawaguchi, K.; Kaifu, N.; Ohishi, M.; Ishikawa, S.I.; Hirahara, Y.; Yamamoto, S.; Irvine, W.M. Observations of cumulene carbenes, H_2CCCC and H_2CCC , in TMC-1. *Publ. Astron. Soc. Jpn.* **1991**, *43*, 607–619.
90. Cabezas, C.; Tercero, B.; Agúndez, M.; Marcelino, N.; Pardo, J.R.; de Vicente, P.; Cernicharo, J. Cumulene carbenes in TMC-1: Astronomical discovery of $l-H_2C_5$. *Astron. Astrophys.* **2021**, *650*, L9. [CrossRef] [PubMed]
91. Langer, W.D.; Velusamy, T.; Kuiper, T.B.H.; Peng, R.M.M.C.; McCarthy, M.C.; Travers, M.J.; Thaddeus, P. First astronomical detection of the cumulene carbon chain molecule H_2C_6 in TMC-1. *Astrophys. J.* **1997**, *480*, L63. [CrossRef] [PubMed]
92. Kimura, Y.; Tanaka, K.K.; Nozawa, T.; Takeuchi, S.; Inatomi, Y. Pure Iron Grains Are Rare in the Universe. *Sci. Adv.* **2017**, *3*, e1601992. [CrossRef]
93. Koelemay, L.A.; Ziurys, L.M. Elusive Iron: Detection of the FeC Radical ($X^3\Delta_1$) in the Envelope of IRC + 10216. *Astrophys. J. Lett.* **2023**, *958*, L6. [CrossRef]
94. Hawrelak, E.J.; Bernskoetter, W.H.; Lobkovsky, E.; Yee, G.T.; Bill, E.; Chirik, P.J. Square planar vs tetrahedral geometry in four coordinate iron (II) complexes. *Inorg. Chem.* **2005**, *44*, 3103–3111. [CrossRef]
95. Ghosh, A.K.; Neogi, S.; Ghosh, P.; Hajra, A. Synergistic Photoredox and Iron (II) Catalyzed Carbophosphorothiolation of Vinyl Arenes. *Adv. Synth. Catal.* **2023**, *365*, 2271–2278. [CrossRef]
96. Varga, Z.; Verma, P.; Truhlar, D.G. Hyper open-shell states: The lowest excited spin states of o atom, Fe^{2+} ion, and FeF_2 . *J. Am. Chem. Soc.* **2017**, *139*, 12569–12578. [CrossRef]

97. Athanasopoulos, E.; Conradie, J. Substituent effect on the oxidation and reduction of electronically altered iron (II)-terpyridine derivatives-DFT study. *Inorganica Chim. Acta* **2023**, *555*, 121599. [[CrossRef](#)]
98. Chai, J.D.; Head-Gordon, M. Long-Range Corrected Hybrid Density Functionals with Damped Atom-Atom Dispersion Corrections. *Phys. Chem. Chem. Phys.* **2008**, *10*, 6615–6620. [[CrossRef](#)]
99. Young, D. *Computational Chemistry: A Practical Guide for Applying Techniques to Real World Problems*; John Wiley & Sons: Hoboken, NJ, USA, 2004.
100. Fuentealba, P.; Stoll, H.; Von Szentpály, L.; Schwerdtfeger, P.; Preuss, H. On the reliability of semi-empirical pseudopotentials: Simulation of Hartree-Fock and Dirac-Fock results. *J. Phys. B At. Mol. Phys.* **1983**, *16*, L323. [[CrossRef](#)]
101. Fuentealba, P.; Preuss, H.; Stoll, H.; Von Szentpály, L. A proper account of core-polarization with pseudopotentials: Single valence-electron alkali compounds. *Chem. Phys. Lett.* **1982**, *89*, 418–422. [[CrossRef](#)]
102. Pershina, V. Electronic Structure and Properties of Superheavy Elements. *Nucl. Phys. A* **2014**, *944*, 578–613. [[CrossRef](#)]
103. Clark, T.; Chandrasekhar, J.; Spitznagel, G.W.; Von Ragué Schleyer, P. Efficient Diffuse Function-Augmented Basis Sets for Anion Calculations. III. The 3-21+G Basis Set for First-Row Elements, Li-F. *J. Comput. Chem.* **1983**, *4*, 294–301. [[CrossRef](#)]
104. Frisch, M.J.; Trucks, G.W.; Schlegel, H.B.; Scuseria, G.E.; Robb, M.A.; Cheeseman, J.R.; Scalmani, G.; Barone, V.; Petersson, G.A.; Nakatsuji, H.; et al. *Gaussian 16 Revision B.01*; Gaussian Inc.: Wallingford, CT, USA, 2016.
105. Glendening, E.D.; Weinhold, F. Natural resonance theory: I. General formalism. *J. Comput. Chem.* **1998**, *19*, 593–609. [[CrossRef](#)]
106. Reed, A.E.; Weinstock, R.B.; Weinhold, F. Natural Population Analysis. *J. Chem. Phys.* **1985**, *83*, 735–746. [[CrossRef](#)]
107. Zubarev, D.Y.; Boldyrev, A.I. Developing Paradigms of Chemical Bonding: Adaptive Natural Density Partitioning. *Phys. Chem. Chem. Phys.* **2008**, *10*, 5207–5217. [[CrossRef](#)]
108. Zubarev, D.Y.; Boldyrev, A.I. Revealing Intuitively Assessable Chemical Bonding Patterns in Organic Aromatic Molecules via Adaptive Natural Density Partitioning. *J. Org. Chem.* **2008**, *73*, 9251–9258. [[CrossRef](#)] [[PubMed](#)]
109. Becke, A.D.; Edgecombe, K.E. A Simple Measure of Electron Localization in Atomic and Molecular Systems. *J. Chem. Phys.* **1990**, *92*, 5397–5403. [[CrossRef](#)]
110. Lu, T.; Chen, F. Multiwfn: A Multifunctional Wavefunction Analyzer. *J. Comput. Chem.* **2012**, *33*, 580–592. [[CrossRef](#)] [[PubMed](#)]
111. Limon, P.; Miralrio, A.; Castro, M. Small Binary Iron-Carbon Clusters with Persistent High Magnetic Moments. A Theoretical Characterization. *Int. J. Quantum Chem.* **2019**, *119*, e25932. [[CrossRef](#)]
112. Redondo, P.; Largo, L.; Barrientos, C. Charged FeC_n Clusters: A Comparison with TMC_n⁺/TMC_n[−] (TM = Sc, Ti, V, Co and Zn, n = 1–8) Systems. *J. Chem. Phys.* **2009**, *364*, 1–13. [[CrossRef](#)]
113. Fan, J.; Lou, L.; Wang, L.-S. FeC_n[−] and FeC_nH[−] (n = 3,4): A Photoelectron Spectroscopic and Density Functional Study. *J. Chem. Phys.* **1995**, *102*, 2701–2707. [[CrossRef](#)]

Disclaimer/Publisher’s Note: The statements, opinions and data contained in all publications are solely those of the individual author(s) and contributor(s) and not of MDPI and/or the editor(s). MDPI and/or the editor(s) disclaim responsibility for any injury to people or property resulting from any ideas, methods, instructions or products referred to in the content.